Report
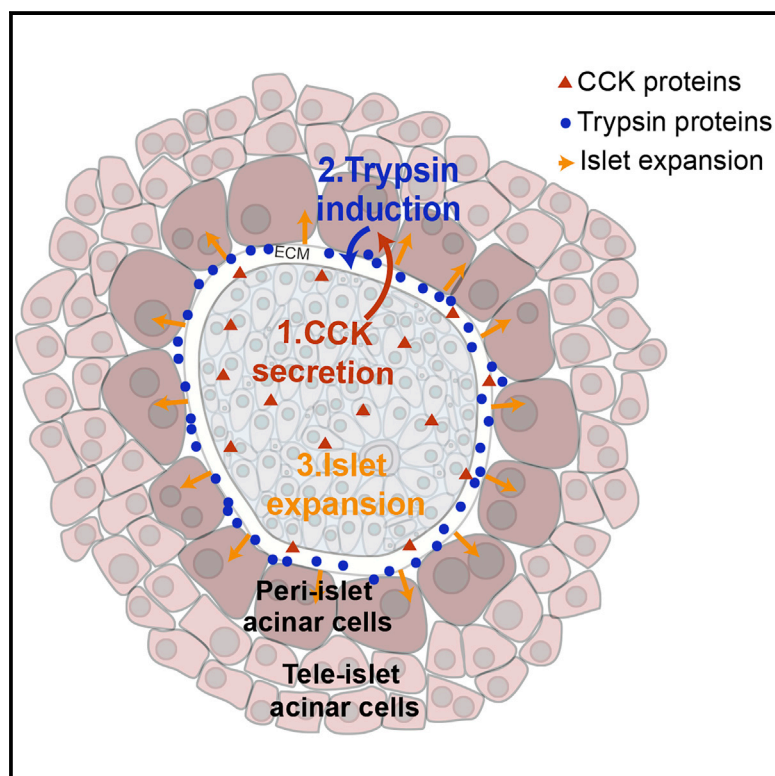
Zonation of Pancreatic Acinar Cells in Diabetic Mice

Graphical Abstract

Authors

Adi Egozi, Keren Bahar Halpern,
Lydia Farack, Hagar Rotem,
Shalev Itzkovitz

Correspondence

shalev.itzkovitz@weizmann.ac.il

In Brief

Egozi et al. identify a zonated gene expression signature of pancreatic acinar cells in diabetic mice. Peri-islet acinar cells elevate trypsin genes. This expression signature is regulated by islet-derived CCK and may be relevant for islet expansion.

Highlights

- Pancreatic acinar cells exhibit a zonated gene expression signature in db/db mice

- Peri-islet acinar cells upregulate trypsin genes and mTOR activity

- Islet-derived CCK induces the zonated acinar gene expression signature

- Exocrine-endocrine crosstalk may be relevant to islet expansion

CellPress

Report

Zonation of Pancreatic Acinar Cells in Diabetic Mice

Adi Egozi,[1] Keren Bahar Halpern,[1] Lydia Farack,[1] Hagar Rotem,[1] and Shalev Itzkovitz[1,2,*]
[1]Department of Molecular Cell Biology, Weizmann Institute of Science, Rehovot 7610001, Israel
[2]Lead Contact
*Correspondence: shalev.itzkovitz@weizmann.ac.il
https://doi.org/10.1016/j.celrep.2020.108043

SUMMARY

The islets of Langerhans are dynamic structures that can change in size, number of cells, and molecular function in response to physiological and pathological stress. Molecular cues originating from the surrounding "peri-islet" acinar cells that could facilitate this plasticity have not been explored. Here, we combine single-molecule transcript imaging in the intact pancreas and transcriptomics to identify spatial heterogeneity of acinar cell gene expression. We find that peri-islet acinar cells exhibit a distinct molecular signature in db/db diabetic mice that includes upregulation of trypsin family genes and elevated mTOR activity. This zonated expression program seems to be induced by CCK that is secreted from islet cells. Elevated peri-islet trypsin secretion could facilitate the islet expansion observed in this model via modulation of the islet capsule matrix components. Our study highlights a molecular axis of communication between the pancreatic exocrine and endocrine compartments that may be relevant to islet expansion.

INTRODUCTION

The endocrine pancreas, composed of the islets of Langerhans, is a dynamic structure that can change in size, number of cells, and function in response to physiological and pathological stress. In states of systemic insulin resistance, such as those observed in the metabolic syndrome or pregnancy, islets exhibit substantial changes that result in higher insulin secretion (Gunasekaran and Gannon, 2011). These changes include the induction of insulin by individual beta cells, an increase in beta cell size (hypertrophy), and an increase in beta cell numbers (hyperplasia). Understanding the molecular cues that facilitate such islet plasticity is important, since they may identify potential avenues to stimulate beta cell expansion. Different studies have highlighted systemic and intrinsic factors that facilitate beta cell expansion (Nielsen et al., 2001). Other studies have highlighted signals in the islet microenvironment, specifically from pericytes, that induce beta cell state and proliferative potential (Sakhneny et al., 2018). The potential involvement of acinar cells in islet expansion has not been explored.

The islets of Langerhans are embedded in the exocrine pancreas, which is predominantly composed of acinar cells. Acinar cells secrete digestive enzymes into pancreatic ducts that drain into the small intestine. Recent work has suggested that acinar cells are not identical, but rather show heterogeneous gene expression (Tosti et al., 2019). Acinar cells in close proximity to the islet, called "peri-islet" acinar cells, have been shown to be morphologically and functionally different from "tele-islet" acinar cells that are farther away (Adelson and Miller, 1989; Anzi et al., 2018; Hellman et al., 1962; Malaisse-Lagae et al., 1975; White and Swartz, 1980). Some of these differences, for example, cell size, have been attributed to the elevated levels of insulin, which could locally diffuse into the pancreas parenchyma (Hellman et al., 1962). However, technical limitations impeded the identification of differences in gene expression between peri-islet and tele-islet acinar cells. Since the quality of mRNA extracted from the pancreas is notoriously low, *in situ* approaches to image mRNA have largely been unsuccessful. Here, we apply a recently developed method for single-molecule fluorescence *in situ* hybridization (smFISH) in the intact pancreas (Farack et al., 2019; Farack, 2020) to explore whether acinar gene expression is zonated (Halpern et al., 2017; Moor et al., 2018), namely, whether the molecular identity of acinar cells changes as a function of their distance from the islets of Langerhans. We uncover a zonated gene expression signature of trypsin genes in diabetic mice. This signature may be induced by islet CCK and could facilitate islet expansion.

RESULTS

smFISH in the Intact Pancreas Reveals Acinar Zonation in db/db Mice

To address potential zonation of acinar cells we chose to focus on adult db/db mice (9–17 weeks). These mice have been shown to be highly insulin resistant and to exhibit substantial islet expansion (Coleman, 1978; Hummel et al., 1966). These changes could result in higher levels of morphogens originating in the islet, which could in turn result in changes in the molecular identities of peri-islet acinar cells.

We examined pancreatic tissues from 9- to 17-week-old B6.BKS(D)-Leprdb/J db/db mice. These mice were shown to be hyperinsulinemic and hyperglycemic (Coleman, 1978; Table
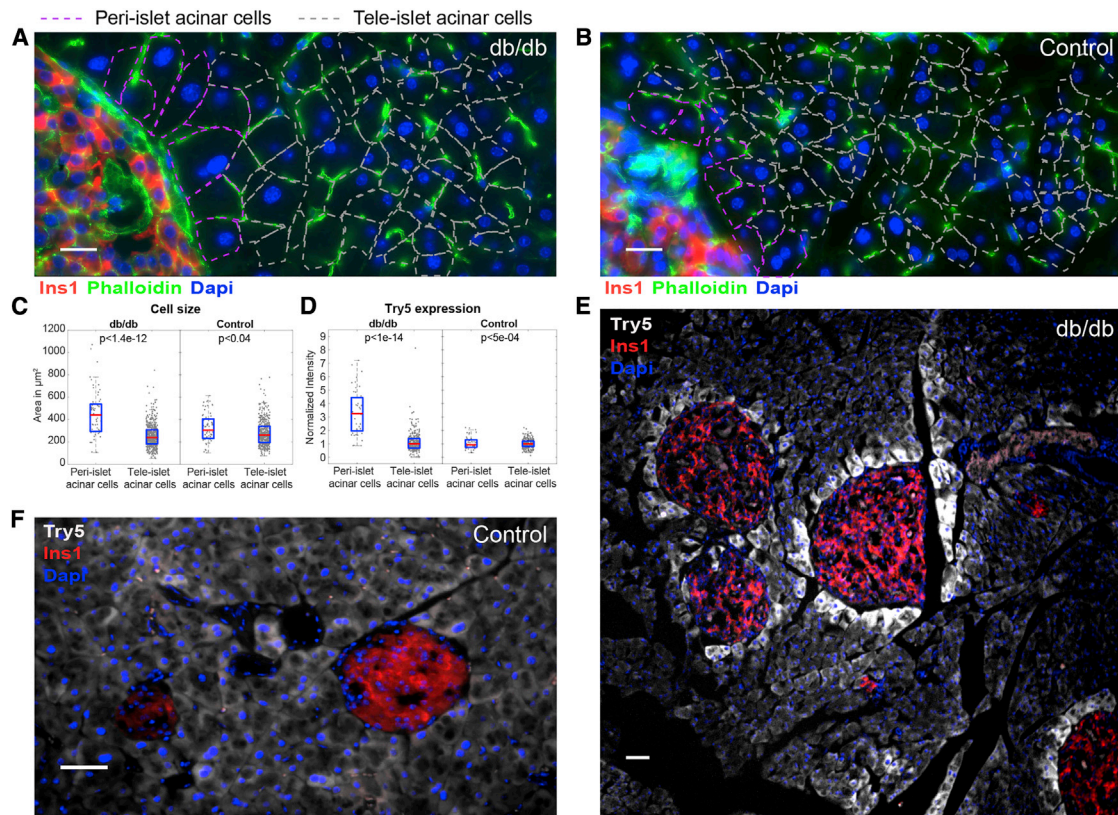
Figure 1. Zonation of Acinar Cells in db/db mice

(A and B) Peri-islet acinar cells (purple dashed lines) are significantly larger than tele-islet acinar cells (gray dashed lines) in db/db mice (A) and to a lesser extent in control mice (B). Red is *Ins1* mRNA, the membrane is stained by phalloidin (green), and nuclei are stained by DAPI (blue). Scale bars, 20 μm.

(C) Quantification of acinar cell size (10 islets from 5 mice, p < 1.4e-12 in db/db mice, p < 0.04 in control mice).

(D) Quantification of peri-islet acinar cell zonation of *Try5* in db/db and control mice (10 islets from 5 mice, p < 1e-14 in db/db mice, p < 5e-04 in controls). Red lines are medians and blue boxes are 25th–75th percentiles. Of 358 cells, 5 are above the maximal shown scale.

(E) *Try5* mRNA (gray) is significantly higher in peri-islet acinar cells compared to tele-islet acinar cells in db/db mice.

(F) *Try5* mRNA (gray) is expressed in a non-zonated manner in control mice.

Islets in (E) and (F) marked by *Ins1* mRNA (red), nuclei stained by DAPI (blue). Scale bars, 50 μm. (A), (B), (E), and (F) are examples of pancreatic tissue of 14- to 17-week-old db/db and control mice.

See also Figures S1, S2, and S3.

S1). We found that peri-islet acinar cells were significantly larger than tele-islet acinar cells, particularly in db/db mice (1.8-fold in db/db mice, p < 1.4e−12, 1.17-fold in control, p < 0.04; Figures 1A–1C). This was in line with previous studies that demonstrated morphological changes in peri-islet acinar cells in this mouse model (Hellman et al., 1962; White and Swartz, 1980).

To identify the potential zonation of gene expression, we used an smFISH protocol optimized for pancreatic tissues (Farack et al., 2019; Farack, 2020). This protocol has been shown to be highly sensitive and quantitative, enabling the detection of individual mRNA molecules as diffraction-limited spots under a fluorescence microscope (Figures S1A and S1B). For highly abundant genes, where single transcripts cannot be resolved, the fluorescence signal intensity correlates with cellular mRNA levels (Farack et al., 2019; Little et al., 2013). We imaged the transcripts of acinar genes encoding key digestive enzymes, including *Try5*, encoding a family member of the serine protease cleaving enzymes (Figures 1D and 1E); *Cel*, encoding carboxyl ester lipase

(Figure S1C); *Cpb1*, encoding carboxypeptidase B1 (Figure S1D); and *Cela2a*, encoding chymotrypsin-like elastase family member 2A (Figure S1E). Notably, *Try5* exhibited significantly higher mRNA levels in peri-islet acinar cells compared to tele-islet acinar cells (Figures 1D, 1E, and S2). These elevated levels of *Try5* in peri-islet acinar cells were not observed in age-matched control mice (Figures 1D, 1F, and S2). We observed a similar zonation of *Try5* in peri-islet acinar cells in BKS.Cg-Dock7m+/+ Leprdb/J db/db mice, an additional insulin-resistant mouse model (Figures S3A–S3C). Our measurements thus indicate that peri-islet acinar cells carry a distinct zonated gene expression signature in db/db mice.

A Global Signature of Peri-islet Acinar Cells Obtained from Isolated Islets

We next sought to obtain a global view of acinar cell zonation in db/db mice. Islet isolation is a common technique for exploring the gene expression signatures of pancreatic endocrine cells
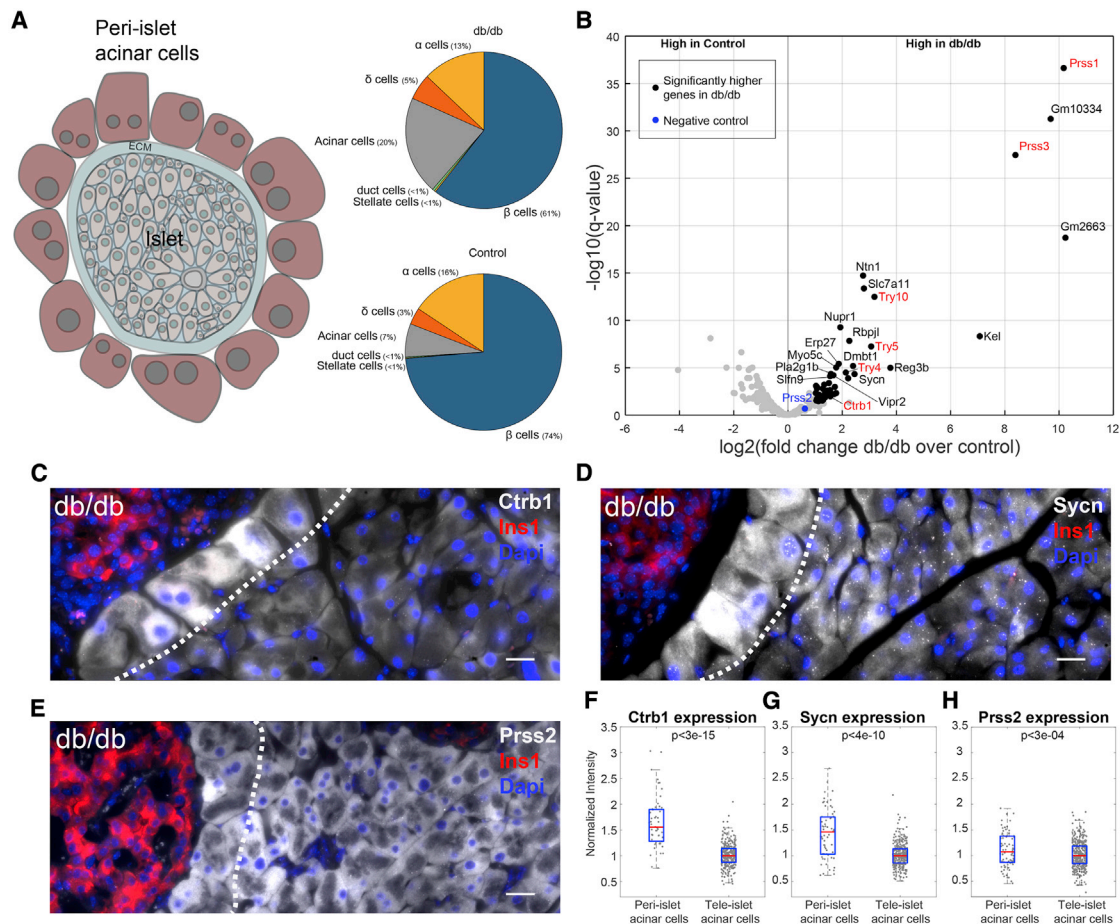
Figure 2. Islet Isolation RNA-Seq Analysis Reveals a Zonated Acinar Cell Signature in db/db Mice

(A) Diagram demonstrating peri-islet acinar cells attached to an isolated islet. Pie charts show the relative fraction of cell-type-specific marker genes in Neelankal John et al. (2018) (see Method Details).

(B) Differential gene expression of acinar-specific genes reveals an upregulation of trypsin genes (red) in islets of db/db mice compared to control mice. The black dots mark genes with log2(fold change) > 1 and q < 0.05. Trypsin genes are in red, except *Prss2* (blue), which is not significantly differentially expressed.

(C and D) smFISH images show higher levels of *Ctrb1* (C) and *Sycn* (D) in peri-islet acinar cells compared to tele-islet acinar cells. Scale bars, 20 μm.

(E) smFISH image shows comparable levels of *Prss2* in peri-islet acinar cells and tele-islet acinar cells.

(F–H) Quantification of smFISH images. Results are based on 10–16 islets from 5–6 mice. p < 3e-15 for Ctrb1, p < 4e-10 for Sycn, p < 3e-04 for Prss2.

Islets in (C)–(E) marked by *Ins1* mRNA (red), nuclei stained by DAPI (blue), and the gene of interest in gray. Scale bars, 20 μm; dashed white lines demarcate peri-islet acinar cells. (C)–(E) are examples of the pancreatic tissue of 14- to 17-week-old db/db mice. The red lines in (F)–(H) are medians and the blue boxes are 25th–75th percentiles.

See also Figure S4 and Tables S2 and S3.

(Jaafar et al., 2019; Neelankal John et al., 2018). The dissociation and extraction protocols used in this procedure could result in residual acinar cells. We hypothesized that such acinar cells would have remained attached to the islet capsule and would thus be enriched for peri-islet cells (Figure 2A). Therefore, exploring the differential gene expression between acinar transcripts in bulk-sequenced islets obtained from db/db mice and control mice could reveal additional zonated acinar genes.

We analyzed datasets of bulk RNA sequencing (RNA-seq) extracted from islets isolated from db/db and control mice (Jaafar et al., 2019; Neelankal John et al., 2018). We used the Tabula Muris dataset (Tabula Muris Consortium, 2018) to assemble a panel of 50 cell-type-specific markers for the main pancreatic

cell types—alpha cells, beta cells, delta cells, stellate cells, duct cells, and acinar cells (Table S2). We found that the extracted islets contained substantial representation of acinar transcripts (20% of the transcripts analyzed in db/db mice and 7% of the transcripts analyzed in control mice; Figure 2A).

We next performed differential gene expression analysis between db/db and control islets (Neelankal John et al., 2018) over acinar-specific genes and identified profound differences in acinar gene expression (Figure 2B; Table S3). Acinar genes induced in db/db mice included all of the trypsin gene family—*Try5* (8.5-fold, q = 6e−8), *Try4* (4.4-fold, q = 3.5e−5), *Try10* (9.2-fold, q = 3.5e−13), *Prss1* (1,162-fold, q = 2.5e−37), *Prss3* (338-fold, q = 3.8e−28), and *Ctrb1* (2.8-fold,
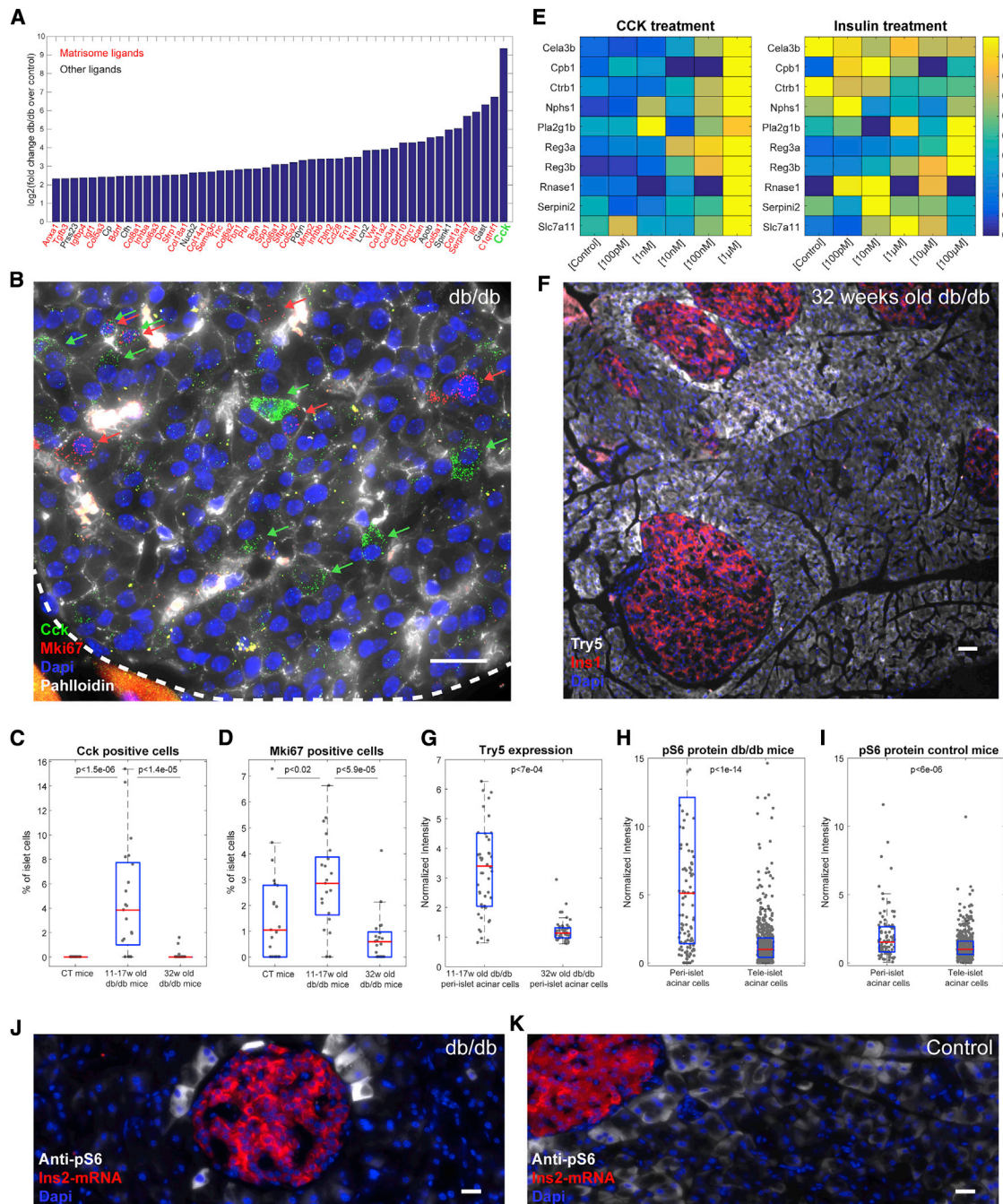
Figure 3. Elevated Intra-islet *Cck* and Acinar Cell Zonation

(A) Bar plot of the fold change of the top 50 ligands between db/db islet and control islets. *Cck* is marked in green and the matrisome ligands are marked in red.

(B) smFISH image of *Cck* (green dots, positive cells marked by green arrows) and *Mki67* (red dots, positive cells marked by red arrows) in db/db islets. The membrane is stained with phalloidin (gray) and the nuclei are stained by DAPI (blue). Scale bar, 20 μm.

(C and D) Quantification of the fractions of islet cells that are *Cck* positive (C, $p < 1.5e{-}06$ between control mice and young db/db mice, $p < 1.4e{-}05$ between young and old db/db mice) and *Mki67* positive (D, $p < 0.02$ between control mice and young db/db mice, $p < 5.9e{-}05$ between young and old db/db mice). The data include 3 mice from each condition and 7 islets for each mouse.

(E) Heatmap of upregulated genes in CCK-exposed AR42J cells and insulin-exposed AR42J cells. Shown are all of the acinar genes that were induced by either CCK or insulin and also zonated *in vivo*. For each gene, the expression is normalized to the maximum across all of the hormone concentrations.

(F) smFISH staining of a 32-week-old db/db mouse, demonstrating the reduction in *Try5* (gray) zonation. Islets are marked by *Ins1* mRNA (red) and the nuclei are stained by DAPI (blue); scale bar, 50 μm.

(legend continued on next page)

q = 0.009)—except *Prss2* (1.6-fold, q = 0.22). Other upregulated genes included the zymogen granule protein *Sycn* (5.5-fold, q = 5e−5). Analysis of a second RNA-seq dataset (Jaafar et al., 2019) revealed high overlap in the induced acinar genes (Figure S4A). Moreover, the peri-islet acinar expression program was highly similar when compared to the db/+ heterozygotes rather than the wild-type (WT) controls (Figure S4B). We validated and quantified the predicted upregulation of some of these genes in peri-islet acinar cells using smFISH, observing substantial upregulation of *Ctrb1* and *Sycn* (>1.4-fold higher expression in peri-islet acinar cells; Figures 2C, 2D, 2F, and 2G). In contrast, *Prss2* was expressed to only slightly (yet significant) higher levels in peri-acinar cells (1.07-fold; Figures 2E and 2H). Our analysis thus indicates that peri-islet acinar cells upregulate a global gene expression signature composed of trypsin genes.

Islet CCK Induces the Peri-islet Zonation Program

Which molecules could induce the peri-islet acinar zonation program we observed in db/db mice? To address this question, we sought to identify ligand molecules (Ramilowski et al., 2015) that are upregulated in db/db islets. We found that *Cck*, encoding the intestinal entero-endocrine hormone cholecystokinin, was the most highly induced ligand (653-fold induction in db/db mice, q = 1.3e−17; Figure 3A; Table S3). Similar increases in intra-islet *Cck* levels were previously shown in ob/ob mice (Lavine et al., 2010). Additional ligands that were significantly upregulated in the db/db mice islets included central matrisome components (Naba et al., 2016), such as collagens and Mmp genes (Figure 3A; Table S3). Using smFISH, we identified abundant expression of *Cck* in db/db islet cells (~4% of islet cells positive for *Cck* in db/db mice and no detectable expression in control islets; Figures 3B and 3C). As expected, db/db islet cells also exhibited higher mRNA levels of the proliferation marker *Mki67* compared to control islets (Figure 3D).

To mechanistically interrogate whether CCK can elicit the peri-islet acinar expression program, we incubated AR42J acinar rat cells (Rosewicz et al., 1992) with increasing levels of CCK or insulin in their medium and sequenced their transcriptomes. Systemic insulin concentrations are ~174 pM (Garzilli and Itzkovitz, 2018) and are expected to be 100-fold higher locally within the peri-islet acinar cells (Unger and Cherrington, 2012). To mimic the high insulin levels that peri-islet acinar cells are exposed to, we therefore exposed cells to concentrations ranging from 100 pM to 100 μM (Figure 3E). These levels were much higher than the insulin levels in the growth medium (7 pM). We focused on acinar-specific genes that were also annotated in the rat

genome. Of these 146 genes, 15 were induced by CCK, and 9 of the 15 were also elevated in peri-islet acinar cells *in vivo* (hypergeometric p = 0.0015; Figure 3E). This set included *Ctrb1*. In contrast, only 3 of the 11 acinar-specific genes that were induced by insulin in the AR42J cell line were elevated *in vivo* (hypergeometric p = 0.32; Figure 3E). Our experiments thus indicate that a significant subset of the db/db peri-islet acinar gene signature is transcriptionally induced by CCK.

We further examined acinar zonation and *Cck* islet expression in older db/db mice (32 weeks old). Unlike the younger db/db mice, *Try5* zonation was significantly decreased in the older mice (p < 7e−4; Figures 3F, 3G, and S2). Notably, the older mice had significantly lower levels of both intra-islet *Cck* mRNA and *Mki67* mRNA (p < 1.4e−5 for *Cck* and p < 5.9e−5 for *Mki67*; Figures 3C and 3D). The correlated decrease in islet *Cck* and peri-islet acinar zonation in older mice further suggest that *Cck* may be inductive for the peri-islet gene expression signature.

Our study identified increases in both peri-islet acinar cell size (Figures 1A and 1C) and the expression of genes encoding trypsin enzymes, which are massively translated and secreted. The mammalian target of rapamycin (mTOR) pathway has been shown to control both cell size (Fingar et al., 2002) and translation rates (Saxton and Sabatini, 2017). We therefore hypothesized that peri-islet acinar cells may exhibit elevated levels of mTOR signaling. We found that the levels of phosphorylated S6 ribosomal protein (pS6), a downstream target of mTOR complex 1 (mTORC1), were significantly higher in peri-islet acinar cells of 9- to 17-week-old db/db mice (5.1-fold, p < 1e−14; Figures 3H and 3J). This zonated mTORC1 activity was also apparent in control mice, although at a significantly less pronounced level (1.5-fold change, p < 6e−06; Figures 3I and 3K). Peri-islet acinar cells in db/db mice therefore exhibit a substantial increase in mTOR signaling.

DISCUSSION

Our study uncovered a zonated gene expression signature in db/db mice consisting of a specific induction of trypsin genes in the layer of acinar cells that surrounds the islets of Langerhans. Previous studies of peri-islet acinar cells hypothesized that insulin that locally diffuses from islets within the pancreatic parenchyma would be the stimulator of peri-islet acinar cell phenotypes such as increased size and protein secretion (Trimble et al., 1985). In contrast, our study supports the role of CCK, a central secretagogue of acinar cells, as a facilitator of acinar cell zonation via three lines of evidence: (1) *Cck* was the most highly induced


(G) Peri-islet *Try5* is significantly more zonated in young versus old db/db mice (p < 7e-04). Of 97 cells, 5 are above the maximal shown scale. The results are based on 9–10 islets from 3–5 mice.

(H and I) Quantification of peri-islet acinar cell zonation of anti-pS6 in db/db mice (H, p < 1e-14) and control mice (I, p < 6e-06). 39 of 683 cells (H) and 2 of 563 cells (I) are above the maximal shown scale. The results are based on 9–15 islets from 3–5 mice.

(J and K) Examples of islets in a db/db mouse (J) and a control mouse (K) stained with anti-pS6 (gray). Islets are marked by *Ins2* mRNA (red) and the nuclei are stained by DAPI (blue); scale bar, 20 μm.

In (C), (D), and (G)–(I), the red lines are medians and the blue boxes are 25th–75th percentiles. (B), (J), and (K) are examples of the pancreatic tissue of 14- to 17-week-old db/db and control mice.

See also Figure S2 and Table S3.
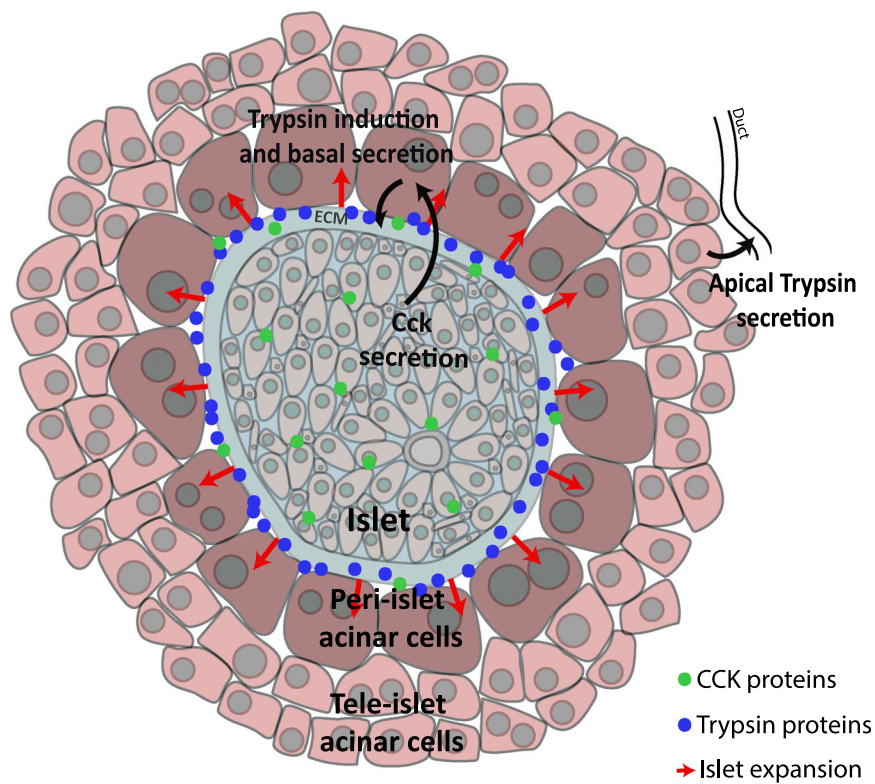
Figure 4. Model for Acinar Cell Zonation in db/db Mice

Islet cells elevate CCK levels (green dots), which elicit a zonated increase in both the expression of trypsin genes in peri-islet acinar cells and their basal secretion (blue dots). Such induction could contribute to islet capsule ECM remodeling, potentially facilitating islet expansion (red arrows).

in protein digestion. Elevated levels of CCK have been shown to lead to mistrafficking of digestive enzymes, inhibition of apical secretion, and abnormal exocytosis redirected to the basolateral plasma membrane (Gaisano et al., 2001; Liang et al., 2017; Scheele et al., 1987; Chen, 2018). Such basal secretion of trypsin has been implicated in cellular damage during pancreatitis (Gaisano et al., 2001). Islets in insulin-resistant animals often expand in size (Chen et al., 2017) to meet the demands of increased insulin production. This increase entails changes in the expression of many matrisome components in the db/db islets (Figure 3A; Table S3). Basal secretion of trypsin from peri-islet acinar cells could facilitate these changes by cleaving capsule extracellular matrix (ECM) proteins (Figure 4). In line with this hypothesis, TAT, a trypsin-like protein, has been shown to contribute to the cell-mediated degradation of ECM in tumors (Koivunen et al., 1991). Trypsin and other proteases have been shown to act synergistically with collagenase in separating islets from the surrounding exocrine tissue (Wolters et al., 1992). Trypsin is also highly potent in dissociating islets and is commonly used in islet digestion protocols (Lu et al., 2017). These effects of trypsin could stem from their breakdown of collagen-binding proteoglycans and glycoproteins (Brandhorst et al., 2009). The mere change in ECM composition could also lead to the observed changes in peri-islet acinar gene expression, as matrix properties affect the gene expression of cells (Lelièvre, 2009). In contrast to this hypothesis, our ex vivo experiment, which assessed acinar cells in culture without the associated ECM, supports the direct role of CCK as the potential inducing factor.

The decline in intra-islet Cck and acinar cell zonation in older db/db mice coincided with a decrease in intra-islet levels of the proliferation marker Mki67 (Figures 3C and 3D). Our study thus suggests an axis of communication whereby expanding islets induce Cck that locally diffuses and is sensed by peri-islet acinar cells. The CCK stimulation gives rise to both transcriptional induction of trypsin genes and, potentially, their basal secretion (Figure 4). It will be interesting to apply dynamic measurements of acinar cell secretion in pancreatic slices (Liang et al., 2017) to assess the ability of peri-islet acinar cells to secrete zymogen basally toward the islet capsule in the contexts of islet expansion studied here.

ligand in the db/db islets (Figures 3A–3C); (2) elevated CCK levels in acinar cell cultures elicit transcriptional changes that overlap the peri-islet acinar gene expression signature that we observed in vivo, an overlap that was not observed when treating cells with insulin (Figure 3E); and (3) a decline in intra-islet Cck expression in older mice coincided with a decrease in acinar zonation (Figures 3C, 3F, and 3G). Moreover, CCK is a potent activator of the mTOR pathway, as previously shown in AR42J cells (Inushima et al., 2001), which could also account for our observed increase in mTOR activity in peri-islet acinar cells in db/db mice (Figures 3H and 3J). Beta cell-secreted CCK has been shown to accelerate the progression of pancreatic ductal cancer in obese mice, supporting the ability of CCK to diffuse and affect the exocrine parenchyma (Chung et al., 2020). Notably, peri-islet acinar cell sizes (Figures 1B and 1C) and pS6 activity (Figures 3I and 3K) were also elevated in control mice compared to tele-islet acinar cells. These zonated patterns, at a stage when Cck is not expressed, indicate that other islet-secreted factors such as insulin may also be important regulators of peri-islet acinar cell identity. Future studies could apply cell-type-specific ablation of Cck in islet cells or its receptor genes in acinar cells under the db/db background to further establish the inductive role of CCK in peri-islet acinar cell zonation.

What could be the functional role of the CCK-induced peri-islet acinar zonation that we observed? Under normal physiology, intestinal Cck that is expressed by entero-endocrine cells stimulates the apical secretion of trypsin and other pancreatic acinar enzymes. These enzymes flow through pancreatic ducts into the small intestine, where they participate

Zonation of gene expression has been demonstrated in several epithelial tissues such as the liver (Halpern et al., 2017), the intestine (Moor et al., 2018), and the kidney (Stewart et al., 2019). Our study demonstrates that the diabetic pancreas also exhibits zonated gene expression, possibly induced by islet-derived CCK. It will be important to explore whether similar zonation exists in other models of insulin resistance, such as high-fat diets and pregnancy, during pancreas development and in humans.

STAR★METHODS

Detailed methods are provided in the online version of this paper and include the following:

- KEY RESOURCES TABLE
- RESOURCE AVAILABILITY
  - Lead Contact
  - Materials Availability
  - Data and Code Availability
- EXPERIMENTAL MODEL AND SUBJECT DETAILS
  - Animal experiments
  - Cell lines
- METHOD DETAILS
  - SmFISH and imaging
  - Immunofluorescence (IF) combined with smFISH
  - AR42J cell line experiment
- QUANTIFICATION AND STATISTICAL ANALYSIS
  - smFISH and IF quantification
  - Islet isolation bulk RNA-Seq analysis
  - AR42J cell line sequencing analysis

SUPPLEMENTAL INFORMATION

Supplemental Information can be found online at https://doi.org/10.1016/j.celrep.2020.108043.

AUTHOR CONTRIBUTIONS

S.I. and A.E. conceived the study. A.E. designed and performed most of the experiments. A.E., K.B.H., and L.F. performed the smFISH experiments and image analysis. A.E. and H.R. performed the cell line experiment. A.E. and S.I. performed the data analysis. S.I. and A.E. wrote the manuscript. All of the authors discussed the results and commented on the manuscript.

DECLARATION OF INTERESTS

The authors declare no competing interests.

REFERENCES

Adelson, J.W., and Miller, P.E. (1989). Heterogeneity of the exocrine pancreas. Am. J. Physiol. 256, G817–G825.

Anzi, S., Stolovich-Rain, M., Klochendler, A., Fridlich, O., Helman, A., Paz-Sonnenfeld, A., Avni-Magen, N., Kaufman, E., Ginzberg, M.B., Snider, D., et al. (2018). Postnatal Exocrine Pancreas Growth by Cellular Hypertrophy Correlates with a Shorter Lifespan in Mammals. Dev. Cell 45, 726–737.e3.

Bagnoli, J.W., Ziegenhain, C., Janjic, A., Wange, L.E., Vieth, B., Parekh, S., Geuder, J., Hellmann, I., and Enard, W. (2018). Sensitive and powerful single-cell RNA sequencing using mcSCRB-seq. Nat. Commun. 9, 2937.

Benjamini, Y., and Hochberg, Y. (1995). Controlling the False Discovery Rate: A Practical and Powerful Approach to Multiple Testing. J. R. Stat. Soc. Ser. B Methodol. 57, 289–300.

Brandhorst, H., Friberg, A., Andersson, H.H., Felldin, M., Foss, A., Salmela, K., Lundgren, T., Tibell, A., Tufveson, G., Korsgren, O., and Brandhorst, D. (2009). The importance of tryptic-like activity in purified enzyme blends for efficient islet isolation. Transplantation 87, 370–375.

Chen, X. (2018). Protein Composition and Biogenesis of the Pancreatic Zymogen Granules. American Pancreatic Association's Pancreapedia. https://www.pancreapedia.org/reviews/protein-composition-and-biogenesis-of-pancreatic-zymogen-granules.

Chen, C., Cohrs, C.M., Stertmann, J., Bozsak, R., and Speier, S. (2017). Human beta cell mass and function in diabetes: recent advances in knowledge and technologies to understand disease pathogenesis. Mol. Metab. 6, 943–957.

Chung, K.M., Singh, J., Lawres, L., Dorans, K.J., Garcia, C., Burkhardt, D.B., Robbins, R., Bhutkar, A., Cardone, R., Zhao, X., et al. (2020). Endocrine-Exocrine Signaling Drives Obesity-Associated Pancreatic Ductal Adenocarcinoma. Cell 181, 832–847.e18.

Coleman, D.L. (1978). Obese and diabetes: two mutant genes causing diabetes-obesity syndromes in mice. Diabetologia 14, 141–148.

Farack, L., et al. (2020). Protocol for Single-Molecule Fluorescence In Situ Hybridization for Intact Pancreatic Tissue. STAR Protocols 1. https://doi.org/10.1016/j.xpro.2019.100007. https://www.sciencedirect.com/science/article/pii/S2666166719300073?via%3Dihub.

Farack, L., Golan, M., Egozi, A., Dezorella, N., Bahar Halpern, K., Ben-Moshe, S., Garzilli, I., Tóth, B., Roitman, L., Krizhanovsky, V., and Itzkovitz, S. (2019). Transcriptional Heterogeneity of Beta Cells in the Intact Pancreas. Dev. Cell 48, 115–125.e4.

Fingar, D.C., Salama, S., Tsou, C., Harlow, E., and Blenis, J. (2002). Mammalian cell size is controlled by mTOR and its downstream targets S6K1 and 4EBP1/eIF4E. Genes Dev. 16, 1472–1487.

Gaisano, H.Y., Lutz, M.P., Leser, J., Sheu, L., Lynch, G., Tang, L., Tamori, Y., Trimble, W.S., and Salapatek, A.M. (2001). Supramaximal cholecystokinin displaces Munc18c from the pancreatic acinar basal surface, redirecting apical exocytosis to the basal membrane. J. Clin. Invest. 108, 1597–1611.

Garzilli, I., and Itzkovitz, S. (2018). Design principles of the paradoxical feedback between pancreatic alpha and beta cells. Sci. Rep. 8, 10694.

Gunasekaran, U., and Gannon, M. (2011). Type 2 diabetes and the aging pancreatic beta cell. Aging (Albany NY) 3, 565–575.

Halpern, K.B., Shenhav, R., Matcovitch-Natan, O., Tóth, B., Lemze, D., Golan, M., Massasa, E.E., Baydatch, S., Landen, S., Moor, A.E., et al. (2017). Single-cell spatial reconstruction reveals global division of labour in the mammalian liver. Nature 542, 352–356.

Hellman, B., Wallgren, A., and Petersson, B. (1962). Cytological characteristics of the exocrine pancreatic cells with regard to their position in relation to the

islets of Langerhans. A study in normal and obese-hyperglycaemic mice. Acta Endocrinol. (Copenh.) *39*, 465–473.

Hummel, K.P., Dickie, M.M., and Coleman, D.L. (1966). Diabetes, a new mutation in the mouse. Science *153*, 1127–1128.

Inushima, K., Okabayashi, Y., Sakaguchi, K., Matsumura, Y., Kimura, S., Inoue, Y., and Kasuga, M. (2001). Cholecystokinin activation of 70-kDa S6 kinase in exocrine pancreas. Dig. Dis. Sci. *46*, 1437–1443.

Jaafar, R., Tran, S., Shah, A.N., Sun, G., Valdearcos, M., Marchetti, P., Masini, M., Swisa, A., Giacometti, S., Bernal-Mizrachi, E., et al. (2019). mTORC1 to AMPK switching underlies β-cell metabolic plasticity during maturation and diabetes. J. Clin. Invest. *129*, 4124–4137.

Koivunen, E., Ristimäki, A., Itkonen, O., Osman, S., Vuento, M., and Stenman, U.H. (1991). Tumor-associated trypsin participates in cancer cell-mediated degradation of extracellular matrix. Cancer Res. *51*, 2107–2112.

Lavine, J.A., Raess, P.W., Stapleton, D.S., Rabaglia, M.E., Suhonen, J.I., Schueler, K.L., Koltes, J.E., Dawson, J.A., Yandell, B.S., Samuelson, L.C., et al. (2010). Cholecystokinin is up-regulated in obese mouse islets and expands beta-cell mass by increasing beta-cell survival. Endocrinology *151*, 3577–3588.

Lelièvre, S.A. (2009). Contributions of extracellular matrix signaling and tissue architecture to nuclear mechanisms and spatial organization of gene expression control. Biochim. Biophys. Acta *1790*, 925–935.

Liang, T., Dolai, S., Xie, L., Winter, E., Orabi, A.I., Karimian, N., Cosen-Binker, L.I., Huang, Y.-C., Thorn, P., Cattral, M.S., and Gaisano, H.Y. (2017). *Ex vivo* human pancreatic slice preparations offer a valuable model for studying pancreatic exocrine biology. J. Biol. Chem. *292*, 5957–5969.

Little, S.C., Tikhonov, M., and Gregor, T. (2013). Precise developmental gene expression arises from globally stochastic transcriptional activity. Cell *154*, 789–800.

Lu, J., Yu, Y., and Ungrin, M. (2017). Enhancing the efficiency of human pancreatic islet dissociation. J. Undergrad. Res. Alberta *6*, 25–28.

Lyubimova, A., Itzkovitz, S., Junker, J.P., Fan, Z.P., Wu, X., and van Oudenaarden, A. (2013). Single-molecule mRNA detection and counting in mammalian tissue. Nat. Protoc. *8*, 1743–1758.

Malaisse-Lagae, F., Ravazzola, M., Robberecht, P., Vandermeers, A., Malaisse, W.J., and Orci, L. (1975). Exocrine pancreas: evidence for topographic partition of secretory function. Science *190*, 795–797.

Moor, A.E., Harnik, Y., Ben-Moshe, S., Massasa, E.E., Rozenberg, M., Eilam, R., Bahar Halpern, K., and Itzkovitz, S. (2018). Spatial Reconstruction of Single Enterocytes Uncovers Broad Zonation along the Intestinal Villus Axis. Cell *175*, 1156–1167.e15.

Naba, A., Clauser, K.R., Ding, H., Whittaker, C.A., Carr, S.A., and Hynes, R.O. (2016). The extracellular matrix: tools and insights for the "omics" era. Matrix Biol. *49*, 10–24.

Neelankal John, A., Ram, R., and Jiang, F.-X. (2018). RNA-Seq Analysis of Islets to Characterise the Dedifferentiation in Type 2 Diabetes Model Mice db/db. Endocr. Pathol. *29*, 207–221.

Nielsen, J.H., Galsgaard, E.D., Møldrup, A., Friedrichsen, B.N., Billestrup, N., Hansen, J.A., Lee, Y.C., and Carlsson, C. (2001). Regulation of beta-cell mass by hormones and growth factors. Diabetes *50* (*Suppl 1*), S25–S29.

Parekh, S., Ziegenhain, C., Vieth, B., Enard, W., and Hellmann, I. (2018). zUMIs - a fast and flexible pipeline to process RNA sequencing data with UMIs. Gigascience *7*, giy059.

Preibisch, S., Saalfeld, S., and Tomancak, P. (2009). Globally optimal stitching of tiled 3D microscopic image acquisitions. Bioinformatics *25*, 1463–1465.

Ramilowski, J.A., Goldberg, T., Harshbarger, J., Kloppmann, E., Lizio, M., Satagopam, V.P., Itoh, M., Kawaji, H., Carninci, P., Rost, B., and Forrest, A.R. (2015). A draft network of ligand-receptor-mediated multicellular signalling in human. Nat. Commun. *6*, 7866.

Robinson, M.D., McCarthy, D.J., and Smyth, G.K. (2010). edgeR: a Bioconductor package for differential expression analysis of digital gene expression data. Bioinformatics *26*, 139–140.

Rosewicz, S., Riecken, E.O., and Wiedenmann, B. (1992). The amphicrine pancreatic cell line AR42J: a model system for combined studies on exocrine and endocrine secretion. Clin. Investig. *70*, 205–209.

Sakhneny, L., Rachi, E., Epshtein, A., Guez, H.C., Wald-Altman, S., Lisnyansky, M., Khalifa-Malka, L., Hazan, A., Baer, D., Priel, A., et al. (2018). Pancreatic Pericytes Support β-Cell Function in a Tcf7l2-Dependent Manner. Diabetes *67*, 437–447.

Saxton, R.A., and Sabatini, D.M. (2017). mTOR Signaling in Growth, Metabolism, and Disease. Cell *168*, 960–976.

Scheele, G., Adler, G., and Kern, H. (1987). Exocytosis occurs at the lateral plasma membrane of the pancreatic acinar cell during supramaximal secretagogue stimulation. Gastroenterology *92*, 345–353.

Schindelin, J., Arganda-Carreras, I., Frise, E., Kaynig, V., Longair, M., Pietzsch, T., Preibisch, S., Rueden, C., Saalfeld, S., Schmid, B., et al. (2012). Fiji: an open-source platform for biological-image analysis. Nat. Methods *9*, 676–682.

Stewart, B.J., Ferdinand, J.R., Young, M.D., Mitchell, T.J., Loudon, K.W., Riding, A.M., Richoz, N., Frazer, G.L., Staniforth, J.U.L., Vieira Braga, F.A., et al. (2019). Spatiotemporal immune zonation of the human kidney. Science *365*, 1461–1466.

Tabula Muris Consortium (2018). Single-cell transcriptomics of 20 mouse organs creates a *Tabula Muris*. Nature *562*, 367–372.

Tosti, L., Hang, Y., Trefzer, T., Steiger, K., Ten, F.W., Lukassen, S., Ballke, S., Kuehl, A.A., Spieckermann, S., Bottino, R., et al. (2019). Single nucleus RNA sequencing maps acinar cell states in a human pancreas cell atlas. bioRxiv. https://doi.org/10.1101/733964.

Trimble, E.R., Bruzzone, R., Gjinovci, A., and Renold, A.E. (1985). Activity of the insulo-acinar axis in the isolated perfused rat pancreas. Endocrinology *117*, 1246–1252.

Unger, R.H., and Cherrington, A.D. (2012). Glucagonocentric restructuring of diabetes: a pathophysiologic and therapeutic makeover. J. Clin. Invest. *122*, 4–12.

White, J.W., and Swartz, F.J. (1980). Changes in polyploidization of exocrine pancreas in db/db diabetic and normal mice. Acta Endocrinol. (Copenh.) *94*, 523–528.

Wolters, G.H., Vos-Scheperkeuter, G.H., van Deijnen, J.H., and van Schilfgaarde, R. (1992). An analysis of the role of collagenase and protease in the enzymatic dissociation of the rat pancreas for islet isolation. Diabetologia *35*, 735–742.

CellPress
OPEN ACCESS

STAR★METHODS

KEY RESOURCES TABLE

REAGENT or RESOURCE	SOURCE	IDENTIFIER
Antibodies		
Rabbit anti-Phospho-S6 Ribosomal	Cell Signaling Technology	Cat. No. 4856; RRID: AB_2181037
Goat anti-Rabbit IgG (Alexa Fluor 647)	Thermo Fisher	Cat. No. A-21245; RRID: AB_2535813
Biological Samples		
Fetal Bovine Serum	Biological Industries	Cat. No. 04-005-1A
Chemicals, Peptides, and Recombinant Proteins		
O.C.T. Compound Cryostat Embedding Medium	Scigen	Cat. No. 4586
Poly-L-lysin solution	Sigma-Aldrich	Cat. No. P8920
Formaldehyde, 37% (w/v)	J.T. Baker	Cat. No. JT2106
PBS, pH 7.4, RNase-free, 10 ×	Ambion	Cat. No. AM9625
Water UltraPure Dnase/RNase-free Molecular Biology	Bio-Lab	Cat. No. 23217723
Proteinase K	Ambion	Cat. No. AM2546
Formamide, deionized, nuclease-free	Ambion	Cat. No. AM9342
Dextran sulfate	Sigma-Aldrich	Cat. No. D8906
E.coli tRNA, Roche	Sigma-Aldrich	Cat. No. R1753
BSA	Ambion	Cat. No. AM2616
Vanadyl- ribonucleoside complex	NEB	Cat. No. S1402S
Cy5 Mono-Reactive Dye Pack	Sigma-Aldrich	Cat. No. PA25001
6-TMRA, SE	Thermo Fisher	Cat. No. C6123
Alexa Fluor 594 carboxylic acid, succinimidyl ester	Thermo Fisher	Cat. No. A20004
DAPI	Sigma-Aldrich	Cat. No. D9542
Alexa Fluor 488 Phalloidin	Thermo Fisher	Cat. No. A12379
ProLong Gold Antifade Mountant	Molecular Probes	Cat. No. P36934
CAS block	Thermo Fisher	Cat. No. 008120
TRI reagent	Sigma-Aldrich	Cat. No. T9424
(Tyr[SO3H]27) Cholecystokinin fragment 26-33 Amide	Sigma-Aldrich	Cat. No. C2175
Insulin	Sigma-Aldrich	Cat. No. I1882
Maxima H -RT	Thermo Fisher	Cat. No. EP0753
dNTPs	Thermo Fisher	Cat. No. R0182
PEG 8000	Sigma-Aldrich	Cat. No. 89510
Exonuclease I	Thermo Fisher	Cat. No. EN0582
AM pure beads	Beckman Coulter	Cat. No. A63881
Terra direct polymerase	Clontech	Cat. No. 639270
Critical Commercial Assays		
Direct-zol RNA Miniprep kit	Zymo Research	Cat. No. R2050
Nextera XT DNA Library Prep Kit	Illumina	Cat. No. FC-131-1024
NextSeq 500 Kits v2 (75 cycles)	Illumina	Cat. No. FC-404-2005
Deposited Data		
RNA sequencing of AR42J cells	This paper	GEO: GSE154533
Islet isolation data	Neelankal John et al., 2018	GEO: GSE107489
Islet isolation data	Jaafar et al., 2019	GEO: GSE132261

Continued

REAGENT or RESOURCE	SOURCE	IDENTIFIER
Tabula Muris dataset	Tabula Muris Consortium, 2018	https://tabula-muris.ds.czbiohub.org/; GEO: GSE109774
Matrisome components data	Naba et al., 2016	http://matrisomeproject.mit.edu/
Ligand-receptor data	Ramilowski et al., 2015	https://doi.org/10.1038/ncomms8866
Experimental Models: Cell Lines		
AR42J	James Dutton	https://www.atcc.org/products/all/CRL-1492.aspx RRID:CVCL_0143
Experimental Models: Organisms/Strains		
B6.BKS(D)-Leprdb/J mice on C57BL/6J genetic background	The Jackson Laboratory	Strain: 000697 | B6 db
BKS.Cg-Dock7m +/+ Leprdb/J on C57BLKS/J genetic background	The Jackson Laboratory	Strain: 000642| BKS db
C57BL/6J mice	The Jackson Laboratory	Strain: 000664 | B6/J
C57BL/6 mice	Envigo	Strain: C57BL/6JOlaHsd
Oligonucleotides		
smFISH probes, see Table S4	This paper	N/A
SINGV6 primer: /5Biosg/ACA CTC TTT CCC TAC ACG ACG C	IDT (Standard Desalting)	N/A
barcoded RT primer	Bagnoli et al., 2018 (Standard Desalting)	N/A
TSO* E5V6NEXT: ACA CTC TTT CCC TAC ACG ACG CrGrG rG	IDT (RNA oligo RNase Free HPLC Purification)	N/A
P5NEXTPT5: AAT GAT ACG GCG ACC ACC GAG ATC TAC ACT CTT TCC CTA CAC GAC GCT CTT CCG* A*T*C* T	IDT (HPLC purification)	N/A
Software and Algorithms		
Stellaris FISH Probe Designer	Biosearch Technologies, Inc., Petaluma, CA	https://biosearchtech.com/products/rna-fish/
R and RStudio v3.6.1	R Consortium	https://rstudio.com/
MATLAB R2016b	MathWorks	https://www.mathworks.com/
ImageM	Lyubimova et al., 2013	N/A
ImageJ 1.52d	Schindelin et al., 2012	https://imagej.nih.gov/ij/; RRID:SCR_003070
MetaMorph software	Molecular Devices, Downington, PA	https://www.biocompare.com/19333-Image-Analysis-Software-Image-Processing-Software/78845-MetaMorphreg-Microscopy-Automation-Image-Analysis-Software/
NIS-Elements software	Nikon Instruments, Melville, NY	https://www.nikon.com/products/microscope-solutions/lineup/img_soft/nis-elements/
edgeR version 3.26.8	Robinson et al., 2010	N/A
bcl2fastq	Illumina	https://support.illumina.com/sequencing/sequencing_software/bcl2fastq-conversion-software.html RRID: SCR_015058
zUMI package	Parekh et al., 2018	N/A

RESOURCE AVAILABILITY

Lead Contact

Further information and requests for resources and reagents should be directed to and will be fulfilled by the Lead Contact, Shalev Itzkovitz (shalev.itzkovitz@weizmann.ac.il).

Materials Availability

This study did not generate new unique reagents.

Data and Code Availability

The accession number for the data reported in this study is GEO: GSE154533.

EXPERIMENTAL MODEL AND SUBJECT DETAILS

Animal experiments

All animal studies were approved by the Institutional Animal Care and Use committee of Weizmann Institute of Science. All C57BL/6 male mice were purchased from Envigo and Jackson Laboratory. Homozygous B6.BKS(D)-Leprdb/J (db/db) male and female mice were purchased from Jackson Laboratory. Homozygous BKS.Cg-Dock7m +/+ Leprdb/J (db/db) male mice were purchased from Jackson Laboratory and used for Figure S3 only. All mice were fed with normal chow *ad libitum* except the mouse in Figure S1A, which was fasted for 9 hours prior to sacrifice. Mice were sacrificed by cervical dislocation. All mice were allowed to acclimatize to the animal facility environment for at least 7 days before being used for experimentation.

B6.BKS(D)-Leprdb/J mice on C57BL/6J genetic background were sacrificed at ages 9-17 weeks and 32 weeks. C57BL/6J were used as controls. BKS.Cg-Dock7m +/+ Leprdb/J mice on C57BLKS/J genetic background were sacrificed at age 14 weeks. Body weight and blood glucose level for db/db and control mice are shown in Table S1.

Cell lines

AR42J male cells were used for culture experiment. Cells were thawed and let to recover in flasks at 37°C for a week before exposed to CCK or insulin. Growth medium used was low-glucose DMEM, 10% FBS, 1% Pen/strep, 1% NEAA, 1% Glutamine.

METHOD DETAILS

SmFISH and imaging

smFISH was performed with a modified smFISH protocol that was optimized for pancreatic tissues as described in Farack et al. (2019), with an extended period of post fixation of 1 hour instead of 15 minutes. In brief, mice were sacrificed and their pancreas was extracted and rinsed with 1XPBS. Pancreas was fixed in 4% Formaldehyde (FA, J.T. Baker, JT2106) in PBS for 3 hours and subsequently agitated in 30% sucrose, 4% FA in PBS overnight at 4°C. Fixed tissues were embedded in OCT (Scigen, 4586). 5-7μm thick sections of fixed pancreas were sectioned onto poly L-lysine coated coverslips and fixed again in 4% FA in PBS for 1 hour followed by 70% Ethanol dehydration for 2h in 4°C. Tissues were treated for 10 min with proteinase K (10 μg/ml Ambion AM2546) and washed twice with 2 × SSC (Ambion AM9765). Tissues were incubated in wash buffer (30% Formamide Ambion AM9342, 2 × SSC) for 3-5 hours and mounted with the hybridization buffer (10% Dextran sulfate Sigma D8906, 30% Formamide, 1 mg/ml E.coli tRNA Sigma R1753, 2 × SSC, 0.02% BSA Ambion AM2616, 2 mM Vanadyl-ribonucleoside complex NEB S1402S) mixed with 1:3000 dilution of probes. Hybridization mix was incubated with tissues for overnight in a 30°C incubator. SmFISH probe libraries (Table S4) were coupled to Cy5, TMR or Alexa594. After the hybridization, tissues were washed with wash buffer containing 50 ng/ml DAPI (Sigma-Aldrich, D9542) for 15 min at 30 °C followed by GLOX buffer (0.4% Glucose, 1% Tris, 10% SSC) containing Phalloidin conjugated to Alexa Fluor 488 (1:500, Thermo Fisher, A12379) for 20 minutes for cell-membrane staining. Probe libraries were designed using the Stellaris FISH Probe Designer Software (Biosearch Technologies, Inc., Petaluma, CA), see Table S4.

Imaging was performed on either Nikon-Ti-E inverted fluorescence microscopes equipped with 100x and 60x oil-immersion objectives and a Photometrics Pixis 1024 CCD camera or Nikon eclipse Ti2 inverted fluorescence microscopes equipped with 100x and 60x oil-immersion objectives and a Photometrics Prime 95B 25MM EMCCD camera. Image stacks were collected with a z spacing of 0.3μm. Image stitching was performed with the fusion mode linear blending and default settings of the pairwise stitching plugin in Fiji (Preibisch et al., 2009; Schindelin et al., 2012). Quantification of smFISH was done using ImageM (Lyubimova et al., 2013).

Immunofluorescence (IF) combined with smFISH

smFISH was performed as described in the section above. At the second day of the protocol before DAPI staining, the tissues were washed twice with 30% WB for 15 minutes at room temperature, then washed 3 times with 1xPBS each for 5 minutes. Blocking using CAS-Block (Blocking solution, Thermo Fisher, 008120) was performed for 80 minutes at room temperature. Tissues were incubated with anti-Phospho-S6 antibody (1:100, Cell Signaling Technology 4856) in blocking solution for 2h at room temperature. Tissues were washed 3 times with 1xPBS each for 5 minutes and incubated with secondary antibody conjugated to Alexa Fluor 647 (1:200, Thermo Fisher, A-21245) for 45 minutes at room temperature. Tissues were next washed 3 times with 1xPBS each for 5 minutes. Cell borders were marked with Phalloidin conjugated to alexa fluor 488 (1:500) and nuclei were stained with 50 ng/ml DAPI before mounting. Imaging was carried out using the same setting as for the smFISH experiments.

AR42J cell line experiment

AR42J cells were obtained from James Dutton. Cells were thawed and let to recover for a week before exposed to CCK or insulin. Growth medium used was low-glucose DMEM, 10% FBS, 1% Pen/strep, 1% NEAA, 1% Glutamine. CCK (Sigma-Aldrich, C2175) was suspended to stock concentration (0.5mM) in NH4OH as specified in manufacturer instruction. Insulin (Sigma-Aldrich, I1882) was suspended to stock concentration (1.7mM) with 0.01 acetic acid in water as specified in manufacturer instruction. Stocks

were diluted to working concentrations in growth medium. Cells were split into 6 well plates and growth medium with the different concentrations of CCK/insulin was added in triplicates after 24 hours. After additional 24 hours, cells were lysed in TRI reagent (Sigma-Aldrich, T9424) for RNA extraction. RNA was isolated by Direct-zol RNA MiniPrep kit (Zymo Research, R2050) according to the manufacturer instructions and processed with the mcSCRBseq protocol with minor modifications (Bagnoli et al., 2018). RT reaction was performed on 20ng of total RNA with a final volume of 10μl (1x Maxima H Buffer, 1mM dNTPs, 2μM TSO* E5V6NEXT, 7.5% PEG8000, 20U Maxima H enzyme, 1μl barcoded RT primer). Amplification step was 14 PCR cycles. Subsequent steps were applied as mentioned in the protocol. Library preparation was performed using Nextera XT kit (Illumina, FC-131-1024) on 0.6ng amplified cDNA. Library final concentration of 2.2pM was loaded on NextSeq 500 (Illumina, FC-404-2005) sequencing machine with the following cycle distribution: 16bp read1, 66bp read2 with a barcode (i7) length of 8bp. Raw files were converted to FASTQ files using bcl2fastq package (Illumina). To obtain the UMI counts, fastq reads were aligned to the rat reference genome (Rnor_6.0.96) using zUMI package (Parekh et al., 2018). Normalized expression tables were obtained by dividing the UMI counts for each gene by the summed UMI counts over all samples.

QUANTIFICATION AND STATISTICAL ANALYSIS

smFISH and IF quantification

In the imaging experiments, peri-islet cells were defined as the first layer of cells surrounding the islet. For each imaging field (islet), Wilcoxon rank-sum tests were used for comparing size / expression among peri-islet and tele-islet cells. Fisher method was used to combine p values among different islets. SmFISH expression values for each imaging field were divided by the median tele-islet cell expression in the field. smFISH size and intensity quantifications (Figures 1C, 1D, and 2F–2H) results were based on 10-16 islet stitches from 5-6 mice. pS6 intensity quantifications (Figures 3H and 3I) results were based on 9-15 islet stitches from 3-5 mice. *Cck* and *Mki67* positive cells analysis was based on 21 islets from 3 mice for each condition (Figures 3C and 3D). *Try5* quantifications on old versus young db/db mice (Figure 3G) were based on 9-10 islet stitches from 3-5 mice. *Try5* quantifications on BKS.Cg-Dock7m +/+ Leprdb/J db/db mice (Figure S3C) were based on 12 islet stitches from 3 mice. Pixel intensities were quantified over 3 μm of the Z stacks, and divided by the segmented cell volume to obtain the mRNA concentration per cell. Intensities were background-subtracted using islet cells. Probe sequences used in this study are described in Table S4. *Cck* and *Mki67* positive cell (Figures 3C and 3D) were defined as cells with more than two cytoplasmic mRNA molecules. For all analysis, arbitrary islets above 70μm in diameter were selected for control mice, and arbitrary islets above 120μm in diameter were selected for B6.BKS(D)-Leprdb/J db/db mice and islets above 100μm in diameter were picked for BKS.Cg-Dock7m +/+ Leprdb/J db/db mice (since islets are smaller in this strain).

Islet isolation bulk RNA-Seq analysis

Bulk islet RNaseq data was taken from Neelankal John et al. (2018) (Figures 2A, 2B, 3A, and S4B) and from Jaafar et al. (2019) (Figure S4A). The tabula Muris dataset (Tabula Muris Consortium, 2018) was used to define genes that are specific to acinar cells. Acinar specific genes were defined as genes with 3-fold higher expression in acinar cells compared to the maximum expression in all other pancreatic cell types (beta, alpha, delta, stellate and ductal cells). Differential gene expression between db/db and control islet transcriptomes were performed with edgeR version 3.26.8 (Robinson et al., 2010). Genes with less than 10 counts were removed. Q-values were computed using the Benjamini-Hochberg false discovery rate correction (Benjamini and Hochberg, 1995). This analysis was performed on all genes (Table S3) as well as on the acinar-specific genes (Figure 2B; Table S3). Ligand and matrisome gene data (Figure 3A; Table S3) were extracted from Table S3 of all genes. To estimate the degree of representation of non-islet transcripts we examined the islet RNaseq expression of a concise subset of 50 cell-type specific genes for each of the 6 cell types considered (Figure 2A; Table S2). To this end, we identified the genes in Tabula Muris with mean expression above 10^{-4} of cellular transcriptome, ranked the ratio between the mean expression in the cell type of interest and the maximal mean expression in any other cell type and maintained the top 50 genes. We computed the relative fraction of the summed expression of each cell-type specific gene set. Tabula Muris dataset was normalized to the sum of UMIs.
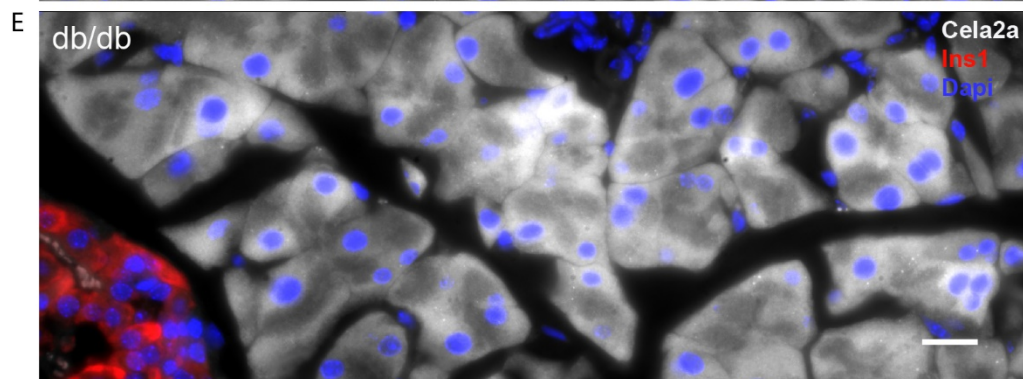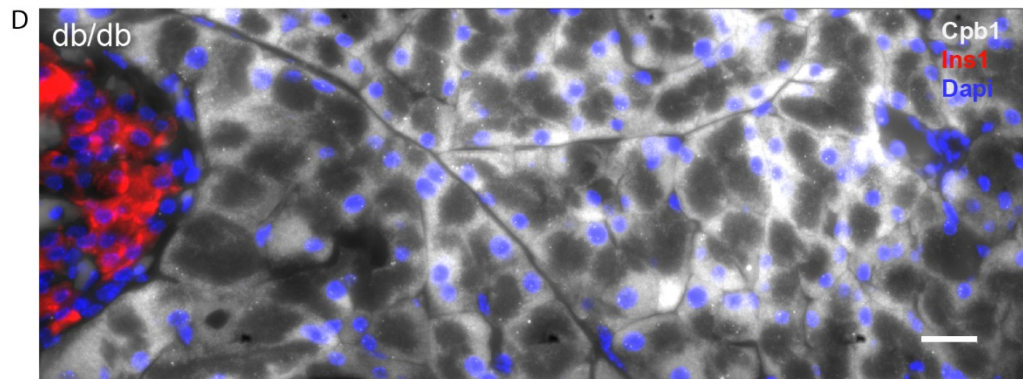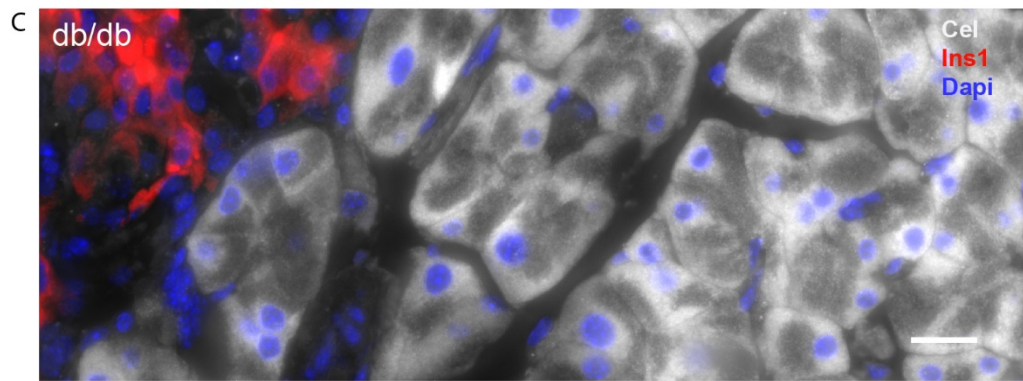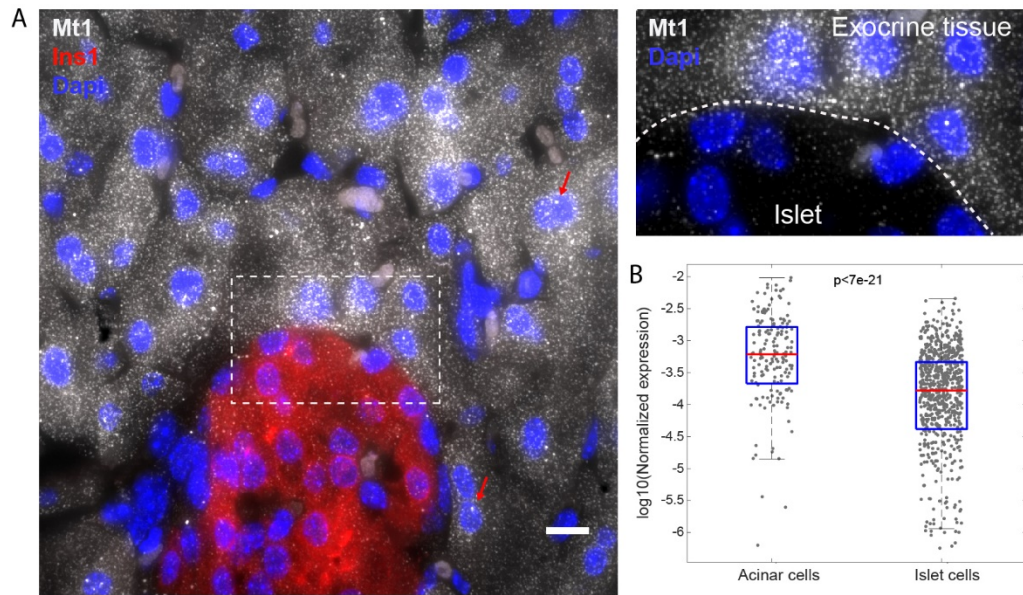
AR42J cell line sequencing analysis

In the AR42J experiment, genes induced by CCK or insulin were defined as genes with maximal expression level observed in the highest hormone dose, that was above 10^{-6} of all transcripts and at least 2-fold higher than the expression with no stimulation. Hypergeometric tests were used to compute the overlap between the genes induced by either hormone and the genes induced in peri-islet cells, defined as acinar genes with levels in db/db islets that were at least 1.5-fold higher than in controls, with q-values < 0.1.
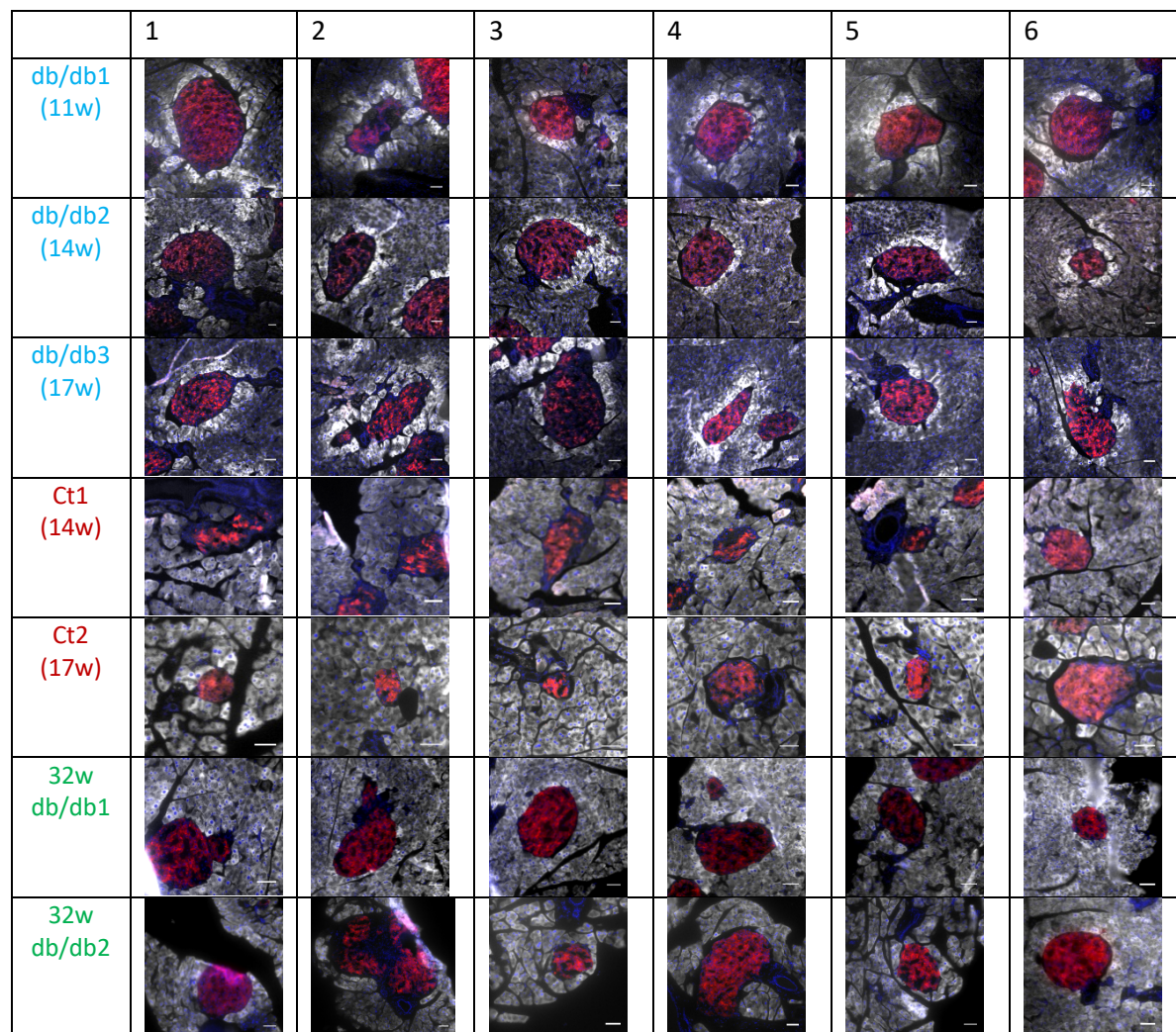
Supplemental Information

Zonation of Pancreatic Acinar Cells

in Diabetic Mice

Adi Egozi, Keren Bahar Halpern, Lydia Farack, Hagar Rotem, and Shalev Itzkovitz

A

Mt1
Ins1
Dapi

Mt1
Dapi

Exocrine tissue

Islet

B

p<7e-21

log10(Normalized expression)

Acinar cells   Islet cells

C

db/db

Cel
Ins1
Dapi

D

db/db

Cpb1
**Ins1**
Dapi

E

db/db

Cela2a
Ins1
Dapi

**Supplementary Figure 1 – smFISH enables quantification of exocrine gene expression in the intact pancreas. Related to Figure 1.** A) smFISH image of *Mt1* mRNA (gray dots) reveals higher expression in acinar cells compared in islet cells (blowup). Red arrows mark transcription sites in the nuclei. B) Quantification of *Mt1* expression from the Tabula Muris single cell dataset (Tabula Muris Consortium et al., 2018) confirms higher expression in acinar cells compared to islet cells (3.7 fold change, p<7e-21). Red lines are medians, blue boxes are 25-75 percentiles. C-E) smFISH images of *Cel* (C), *Cpb1* (D) and *Cela2a* (E) demonstrate non-zonated expression in db/db mice. *Ins1* mRNA in red, Dapi in blue, scale bar-10µm in A and 20µm in C-E.

	1	2	3	4	5	6
db/db1 (11w)						
db/db2 (14w)						
db/db3 (17w)						
Ct1 (14w)						
Ct2 (17w)						
32w db/db1						
32w db/db2						

Supplementary Figure 2 – Montage of *Try5* expression in representative islets from young db/db mice, controls and old db/db mice. Related to Figure 1 and Figure 3. For all images: *Try5* in gray, *Ins1* in red and Dapi in blue. Scale bars-50μm. Islets were selected based on size, regardless of *Try5* gene expression. Color scales are different for each panel and meant to demosntrate the relative intensity between peri-islet and tele-islet acinar cells within each slide.
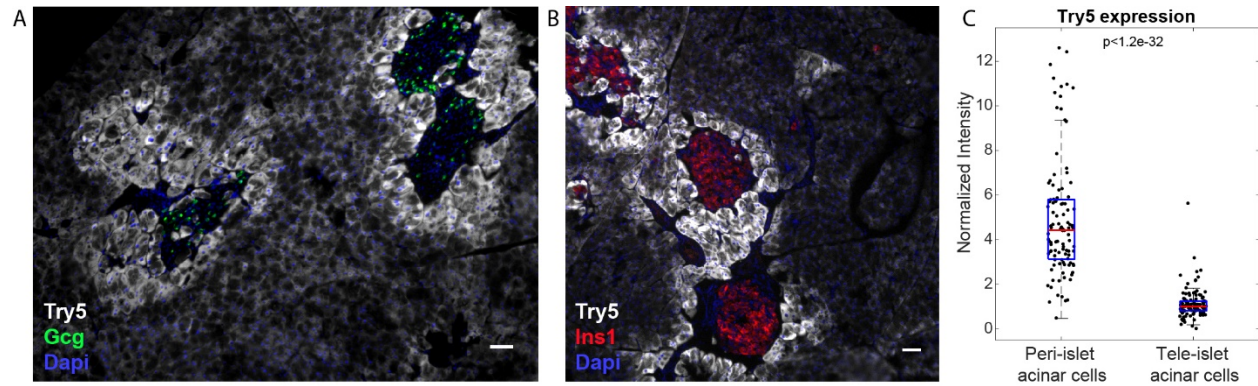
Supplementary Figure 3 – peri-islet acinar zonation of Trypsin is recapitulated in the BKS.Cg-Dock7m+/+ Leprdb/J db/db mouse model. Related to Figure 1. smFISH images from two different 14 weeks old mice. A) *Try5* in gray, *Gcg* in green and Dapi in blue. B) *Try5* in gray, *Ins1* in red and Dapi in blue. Scale bars-50μm. C) *Try5* expression is significantly elevated in peri-islet acinar cells compared to tele-islet acinar cells in BKS.Cg-Dock7m+/+ Leprdb/J db/db mice (12 islets from 3 mice, p<1.2e-32). Red lines are medians, blue boxes are 25-75 percentiles.
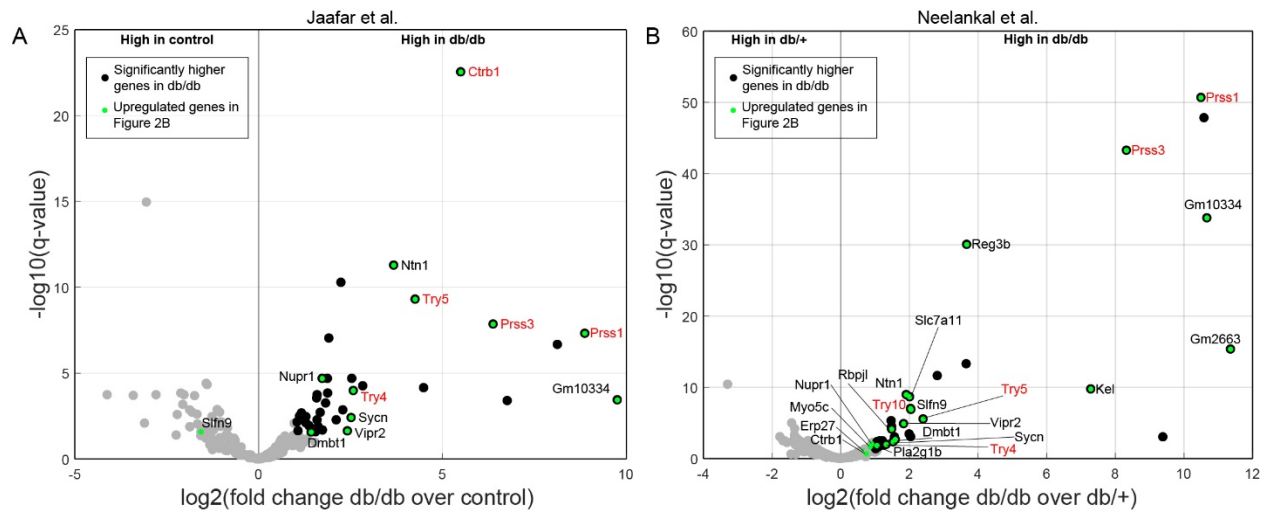
Supplementary Figure 4 – Induction of the peri-islet acinar expression program is similar in another dataset (Jaafar et al., 2019) and when considering db/db vs. db/+ mice (Neelankal John et al., 2018). Related to Figure 2. A) Differential gene expression between acinar transcripts of db/db islets vs. control islets in Jaafar et al. dataset (Jaafar et al., 2019). All genes elevated in Neelankal John et al. (Neelankal John et al., 2018) db/db islets, with the exception of *Slfn9*, are significantly elevated in this dataset as well. B) Differential gene expression between acinar transcripts in db/db islets vs. the heterozygote db/+ islets in Neelankal John et al. dataset (Neelankal John et al., 2018), showing the same set of induced genes as in the comparison with controls (Figure 2B). In both plots, black dots mark genes with log2(fold change) > 1 and q-value<0.05. Green dots are the acinar genes that we found to be significantly induced in db/db islets from Neelankal John et al. (Neelankal John et al., 2018, Figure 2B). Red - trypsin genes.